

Quantified Degeneracy, Entropy and Metal-Insulator Transition in Complex Transition-Metal Oxides

Jae-Hoon Sim¹, Siheon Rye¹, Hunpyo Lee², and Myung Joon Han^{1,3*}

¹*Department of Physics, Korea Advanced Institute of Science and Technology (KAIST), Daejeon 34141, Korea*

²*Department of General Studies, Kangwon National University, Samcheok-si, Kangwon-do 25913, Korea and*

³*KAIST Institute for the NanoCentury, Korea Advanced Institute of Science and Technology, Daejeon 34141, Korea*

(Dated: July 4, 2021)

Understanding complex correlated oxides and their phase transitions has long been a challenge. The difficulty largely arises from the intriguing interplay between multiple degrees of freedoms. While degeneracy can play an important role in determining material characteristics, there is no well-defined way to quantify and to unveil its role in real materials having complicated band structures. Here we suggest a way to quantify the ‘effective degeneracy’ relevant to metal-insulator transition by introducing entropy-like terms. This new quantity well describes the electronic behaviors of transition-metal oxides as a function of external and internal parameters. With 3*d* titanates, 4*d* ruthenates, and 5*d* iridates as our examples, we show that this new effective quantity provides useful insights to understand these systems and their phase transitions. For LaTiO₃/LaAlO₃ superlattice, we suggest a novel ‘degeneracy control’ metal-insulator transition.

Introduction Understanding transition-metal oxides (TMO) and their phase transitions has been a central issue in condensed matter physics and material science. Many of exotic quantum phases of matters are the result of intriguing interplay and competition between the multiple degrees of freedom active in TMO; namely, charge, spin, orbital, and lattice [1]. Estimating the key parameters which represent those degrees of freedom and their couplings is therefore a crucial step. Quantifying other physical parameters such as bandwidth, crystal field, and ‘interactions (*i.e.*, U , U' and J)’ is also often posing a non-trivial task. Depending on which parameter is crucial, the metal-insulator transition (MIT) is described and classified into sub-category of ‘bandwidth control’, ‘filling control’ and ‘dimensionality control’ MIT [1].

Orbital degeneracy can certainly play an important role in determining material characteristics of TMO [2–7]. However, there is no well-defined way to quantify and unveil its role in the cooperation with other physical components of real materials with complicated multi-band structures around Fermi energy (E_F). In this study, we first try to quantify the ‘effective’ orbital degeneracy by introducing entropy-like terms. Then we apply it to real material systems. Our results of 4*d* ruthenates and 5*d* iridates show that this newly-introduced quantity well describes the electronic behavior and provides useful insight to understand MIT. Further, we suggest a novel ‘degeneracy control’ MIT in 3*d* titanate superlattice. The strain-dependent phase diagram and the calculated physical parameters clearly show that the transition is governed mainly by ‘degeneracy’ not by other factors such as bandwidth.

Defining an intuitive and computable physical quantity has been playing central roles in quantum material research. ‘Charge-transfer energy’ for TMO [8] and ‘Chern number’ (or TKNN number) for topological materials [9–11] can be recent examples. Even though both are not

directly measurable in experiments, they certainly provide key information to classify and understand a given type of materials. In this regard, the quantified ‘effective’ degeneracy we suggest here can also be a useful tool to study multi-orbital complex oxides and their phase transitions.

Quantifying Effective Degeneracy In model-based studies, the degree of degeneracy is naturally defined by the energy level difference. For real materials, on the other hand, quantifying degeneracy is not always straightforward due to the complicated band structures which is in the end a result of combinations of many other ‘parameters’ such as crystal field levels and hybridizations. Furthermore we note that the information relevant to MIT is hardly extracted from the ‘bare’ degeneracy represented simply by level differences. With this motivation we define the following quantity:

$$D = \sum_{\mu} S(n_{\mu}). \quad (1)$$

Here the entropy-like term S is given by

$$S(n_{\mu}) = -n_{\mu} \log_2 n_{\mu} - (1 - n_{\mu}) \log_2 (1 - n_{\mu}) \quad (2)$$

where n_{μ} is the eigenvalue of on-site number operator \hat{N} . The matrix elements of \hat{N} can be written as $N_{\alpha\beta} = \frac{1}{N_{\mathbf{k}}} \sum_{\mathbf{km}} \langle \mathbf{km} | \alpha \rangle \langle \beta | \mathbf{km} \rangle$ with orbital indices α and β (*i.e.*, three t_{2g} states in our examples; well represented by Wannier functions), momentum \mathbf{k} , and band index m . Note that $N_{\alpha\beta}$ is calculated from the ‘non-interacting’ Hamiltonian, namely, $U = 0$ paramagnetic band structure, which is the same case with other model parameters to be used to understand MIT such as bandwidth (W) and correlation strength (U) [12, 13]. While the calculation of D at finite U is straightforward, the useful information is mainly contained in D at $U = 0$. The eigenstate $|\mu\rangle$ of the on-site number operator does

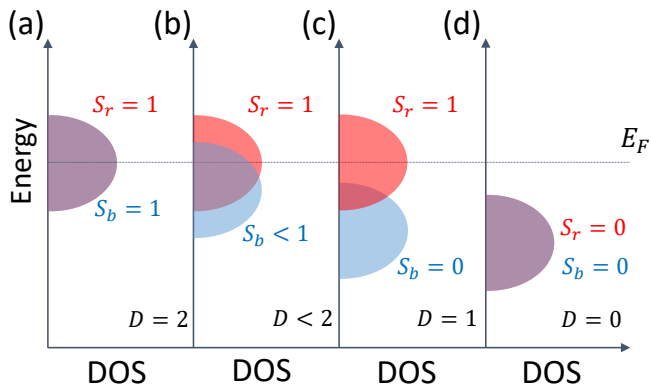


FIG. 1: The behavior of D for some schematic two-orbital electronic structures. In the case of (a), two DOS are fully degenerated and D is maximized, $D = 2$. As two DOS are separated from each other, D is reduced as shown in (b) and (c). As an effective degeneracy (not ‘mere’ degeneracy) D is being reduced when the on-site orbital energy moves far away from E_F . As shown in (d), even if two DOS are ‘fully degenerated’ in the usual sense, the calculated $D=0$ because both states are fully occupied

not need to be any of conventional symmetry states ($|\alpha\rangle$), and can be expressed as the superposition of them [14]. S is maximized ($S = 1$) at half-filling ($n_\mu = 0.5$) and minimized ($S = 0$) when the orbital is fully occupied ($n_\mu = 1$) or unoccupied ($n_\mu = 0$). D reflects the number of orbital states at E_F and thus carries similar information with degeneracy. At the same time, D is clearly different from ‘mere’ degeneracy. The number of states is weighted by taking the band position into account with respect to E_F . As a result, D magnifies the information relevant to MIT. In this sense, D can be called as ‘effective degeneracy’. On the other hand, as obvious from Eq. (2), D measures a certain type of entropy being regarded as ‘effective entropy’. For more discussion of its physical meaning, see Supplemental Material [14].

In order to see how this new quantity works, let us consider a schematic situation presented in Fig. 1. Physically, degeneracy should be largest when the two bands (assumed to have same bandwidths and shapes) are located at the same energy; see Fig. 1(a). It is gradually lifted as two levels become differentiated. Suppose that the band structure evolves from Fig.1(a) to (b) and (c) by any parameter change. S_b (corresponding to one of the two bands; blue colored) is gradually reduced from $S_b=1$ (Fig.1(a)) to $S_b=0$ (Fig.1(c)) while another band (red colored) does not move and S_r is unchanged. When the two density of states (DOS) are identically overlapped with each other (Fig. 1(a)), D is maximized, $D = 2$. When the DOS overlap is minimized (Fig. 1(c)), D is minimized, $D = 1$. Therefore D carries the similar infor-

mation with degeneracy in the usual sense. At the same time, however, D is different from ‘mere degeneracy’ as clearly shown in Fig. 1(d). The calculated D of Fig. 1(d) is zero even though two DOS are fully overlapped. This feature demonstrates that D is defined to represent the ‘effective’ degeneracy or effective entropy of the bands near E_F relevant to MIT. In fact, both DOS in Fig.1(d) are not relevant to MIT since they are fully occupied and far away from E_F .

D works for more general cases. Consider M orbitals whose on-site energies are given by ε ’s near E_F (i.e., $|\varepsilon - E_F| \ll W$ (bandwidth)). For two states per orbital (occupied and unoccupied), the number of configurations is given by $\Omega \sim 2^M$ and $M \sim \log_2 \Omega$. In the case of single electron per site, $D(M) = M \log_2 M - (M - 1) \log_2 (M - 1)$ from $n_\alpha = 1/M$. While $D(M)$ is not equal to but less than M (e.g., $D \sim 3.90$ for $M = 6$), it provides an acceptable measure of degeneracy or entropy for this given model in a general sense.

Applications to Real Materials The usefulness of this new quantity can be more clearly seen with real examples. In the below, we take three different systems of $3d$, $4d$, and $5d$ TMO in which the degeneracy is changed by the internal as well as external parameters. Also, our example sets include both strongly (titanate and iridate; Mott insulators) and moderately correlated (ruthenate in bulk; metals) electron systems. In the below, while we define the standard deviation (σ) of Gaussian fitted DOS as the bandwidth, we confirm that the use of Wannier function or Lorentzian fitting does not change any of our conclusions.

Ruthenates In this subsection we apply our ‘effective degeneracy’ or ‘effective entropy’ to ruthenate thin films. Recently SrRuO₃ (SRO-113) has attracted significant research attention due to its intriguing phase transitions observed as the film thickness is reduced [15–19]. While bulk SRO-113 is a ferromagnetic (FM) metal, its thin film phase is known to become insulating [15–18] and presumably antiferromagnetic (AFM) [16, 20, 21]. Critical thickness and the concomitance of MIT and magnetic transition still remain unclear [15–19].

Fig. 2(a) and (b) shows the projected DOS for 1-layer ($n=1$) and 3-layer ($n=3$) film, respectively. As expected, the Ru- t_{2g} states are more degenerate in $n=3$ being closer to 3-dimensional cubic bulk situation in which the three are completely degenerate. On the other hand, in $n=1$, d_{xy} state is noticeably different from $d_{yz, zx}$.

Here we first note that this electronic structure change is well described by D in a quantitative manner. As shown in Fig. 2(c), the calculated D is gradually increased as n increases being consistent with the intuition and the band structure result. It shows that the newly-defined quantity, D , works reasonably well for describing the realistic band structure change. Furthermore, our result has a meaningful implication regarding the origin of observed MIT as a function of thickness; not only band-

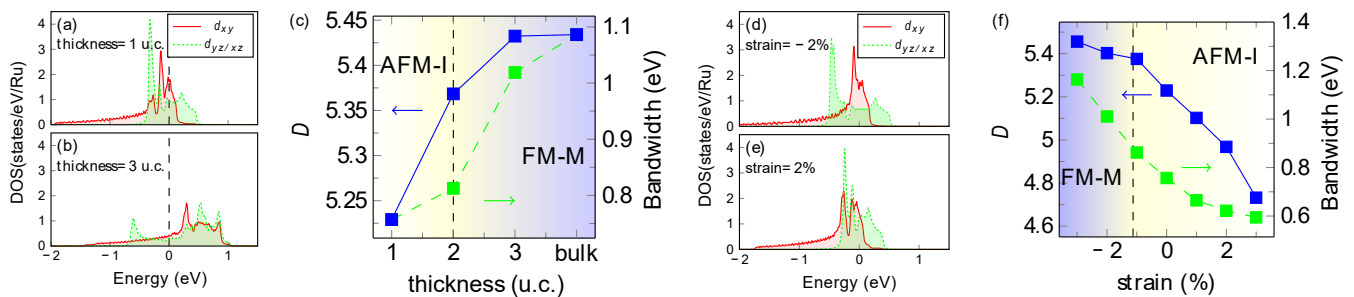


FIG. 2: (a, b) The calculated DOS projected onto Ru- t_{2g} states for (a) $n=1$ and (b) $n=3$ with zero strain. The vertical dashed lines refer to E_F . (c) The calculated D (blue; left side) and bandwidth (green dashed line; right side) as a function of film thickness, n . A transition from FM metal (FM-M; blue-colored) to AFM insulator (AFM-I; yellow-colored) occurs at the thickness of $n=2-4$. (d, e) The calculated DOS projected onto Ru- t_{2g} states for 1-unitcell-thick SRO-113 film with (d) -2% compressive and (e) $+2\%$ tensile strain. (f) The calculated D and bandwidth as a function of strain. At around -1% compressive strain, there is a phase transition from FM-M (blue-colored) to AFM-I (yellow-colored). The DOS, D , and bandwidth are calculated from non-spin-polarized ($U=0$) results while the phase diagrams are constructed from spin-polarized GGA calculations.

width (and/or dimensionality)[19, 21] but also degeneracy plays the role in this transition.

The usefulness of D is further demonstrated in the strain-dependent transition. Fig. 2(d) and (e) presents projected DOS for 2% compressive and tensile strained mono-layer thin film, respectively. We note that in this case the degree of degeneracy is not clearly seen without calculating D . The calculated D as a function of strain is presented in Fig. 2(f) showing that D is gradually decreased as the more tensile strain is applied. In this sense the DOS of Fig. 2(d) is more ‘degenerate’ than that of Fig. 2(e). This example demonstrates that, even when the intuitive conclusion is not likely reached, D extracts the desired information.

Our result shows that D is not ‘mere degeneracy’ in the usual sense but reflects the other factors relevant to MIT. According to Eq. (1) the states near E_F contribute more to D than the other states away from E_F . Importantly, the decreasing trend of D as a function of strain is consistent with the decreasing metallicity. It is known that the system becomes more insulating in the tensile strain regime and more metallic in the compressive strain [21]. In this regard, D represents an ‘effective’ degeneracy or entropy carrying the quantitative information physically relevant to MIT. In the case of DOS in Fig. 2(d), the prominent d_{xy} peak developed around E_F is responsible for larger D (See Supplementary [14]).

Iridates The second example is Sr_2IrO_4 (SIO-214) in which the degeneracy is lifted not by external parameters such as strain and thickness but by spin-orbit coupling (SOC). SIO-214 is known as a ‘relativistic Mott’ insulator in the sense that SOC plays the key role to induce Mott gap [22, 23]. Due to the large crystal field and SOC, Ir- t_{2g} states split into so-called ‘ $j_{\text{eff}}=3/2$ ’ quartet and ‘ $j_{\text{eff}}=1/2$ ’ doublet. Whereas different pictures have been discussed

[24–30], still quite prevailing is that the main role of SOC is to reduce the bandwidth making relatively small U be enough to open the gap [23, 31, 32].

Here we show that the calculation of D supplements the understanding of Mott gap formation. Let us first note that SOC can not only reduce the bandwidth but also lift the degeneracy. This possibility has been speculated in the context of reminiscing about multi-orbital Hubbard model studies [28–30]. However, it could not be discussed quantitatively and therefore not examined systematically in comparison to other possibilities [24–27]. Further, a significant amount of hybridization between $j_{\text{eff}}=1/2$ and $3/2$ has been noted in the literature [28, 32, 33], which render the simple model analysis more difficult.

Fig. 3(a) and (b) shows the projected DOS with and without SOC, respectively, and the calculated bandwidth is presented in Fig. 3(c) as a function of SOC strength (λ). In the range of $0 \leq \lambda \leq 0.5$ eV, the bandwidth is not significantly reduced. Rather, our estimation shows a slight enhancement of bandwidth at the realistic $\lambda=0.479$ eV. In fact, the bandwidth reduction by SOC is not quite clearly seen in the calculated DOS itself. Fig. 3(a) and (b) show that the bandwidth of $j_{\text{eff}}=1/2$ ($\lambda=0.479$ eV) can be regarded as being comparable with that of t_{2g} ($\lambda=0$ eV). Thus, it is difficult to conclude that the gap of SIO-214 is attributed to the bandwidth reduction by SOC.

Our new quantity provides useful insight on this issue. The calculated D is presented in Fig. 3(c) whose decreasing trend clearly shows that the effective degeneracy is gradually lifted by SOC. Together with the estimated critical U_c , which follows the same decreasing trend with D (Fig. 3(d)), our results indicate that lifting degeneracy is the main effect of SOC for the gap formation; SIO-214

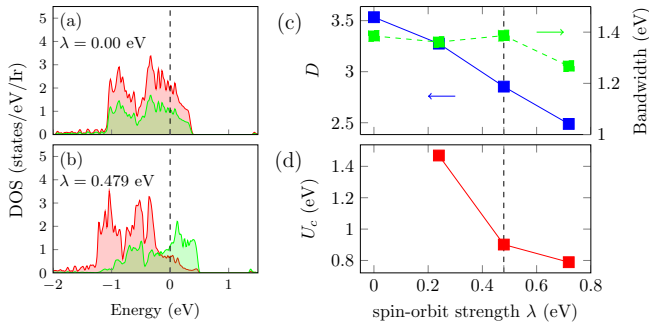


FIG. 3: (a, b) The calculated DOS projected onto so-called j_{eff} states (a) without and (b) with SOC. The red and green colored states represent $j_{\text{eff}} = 3/2$ and $1/2$, respectively. The vertical dashed lines correspond to E_F (c) The calculated bandwidth (green dashed line; right side) of $j_{\text{eff}} = 1/2$ states and D (blue; left side) as a function of λ . Bandwidth are estimated from Gaussian fitting. The realistic value of $\lambda=0.479$ eV is denoted by the vertical dashed lines. (d) The calculated critical U_c value as a function of λ .

may still be regarded as a ‘relativistic Mott’ insulator, but the major role of SOC is not to reduce bandwidth but to lift degeneracy.

Titanates and degeneracy control MIT The final example is a superlattice made of a classical Mott insulator. The material property of $\text{LaTiO}_3/\text{LaAlO}_3$ (LTO/LAO) is an important issue by itself since previous studies show that the electronic and magnetic property are notably different from bulk LTO due to confinement effect [34]. Previous DFT+ U calculations show that FM spin and antiferro orbital order is stabilized [35]. However, no further study has been reported especially using the more advanced techniques beyond static DFT+ U , and a part of experimental observations is still not clearly understood [34]. Our DMFT (dynamical mean-field theory) phase diagram is presented in Fig. 4(a). Paramagnetic insulating (PM-I) phase is clearly identified at high temperature and large U regime, which cannot be addressed by static approximations. The calculated spectral function $A(\mathbf{k}, \omega)$ is presented in Fig. 4(b). Coherent features is noticed below E_F [36] and the correct insulating nature is observed with Γ -point gap of 0.48 eV. This gap size is larger than the bulk LTO optical gap (~ 0.2 eV) being consistent with the conductivity data on $(\text{LTO})_{1,2,3}/(\text{LAO})_5$ which reports that the lowest energy excitation is gradually moving toward the higher frequency as the LTO layer thickness is reduced [34]. At a realistic value of $U = 3$ eV for the superlattice [35, 37], the magnetic transition between ferromagnetic (FM-I) and PM-I occurs at $T_c \simeq 12.5\text{meV}$ in good agreement with the total energy difference by GGA+ U [35]. Overall, our DMFT results in large- U and low- T limit are consistent with

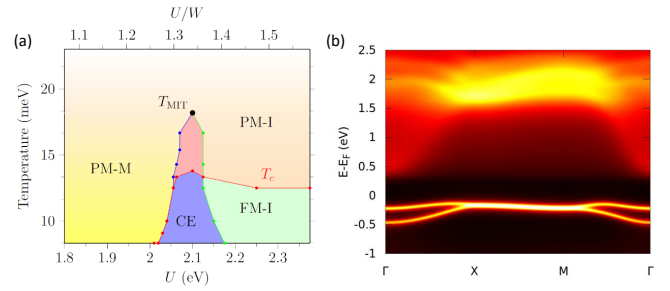


FIG. 4: (a) The U - T phase diagram. The red line indicates the transition from the paramagnetic (PM) to the ferromagnetic (FM) phase. The blue and green lines refer to the transition from metallic-to-insulating, and the insulating-to-metallic state, respectively. CE denotes the coexistence region indicating the first-order transition with an end point at T_{MIT} . (b) The calculated spectral function $A(\mathbf{k}, \omega)$ projected onto Ti with $U = 3$ eV and at $T = 8.3$ meV.

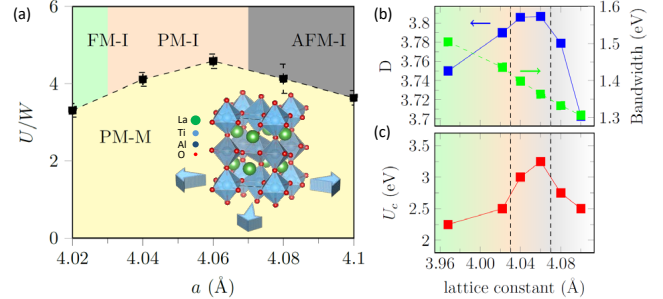


FIG. 5: (a) Strain-dependent DMFT phase diagram in which the dashed line indicates the metal-insulator phase boundary. The metallic region (yellow colored) is enhanced at $a=4.06\text{\AA}$ which corresponds to the degeneracy maximum point. (Inset) Schematic figure for the ‘strain engineering’ of LTO/LAO superlattice. (b) The calculated D (blue; left side) and bandwidth (green dashed line; right side) as a function of in-plane lattice constant. As the more tensile strain applied the bandwidth is gradually decreased as expected. On the other hand, the D is first increased and then decreased with a maximum value at $a=4.06\text{\AA}$. (c) The critical value of U_c as a function of in-plane lattice parameter shows the same trend with D , suggesting that this phase transition is governed mainly by degeneracy.

static DFT+ U calculations.

Now we consider the strain dependence and ‘degeneracy control’ MIT. Fig. 5(a) presents the phase diagram as a function of in-plane lattice parameter. Note that metallic region (yellow) is enlarged at around $a=4.06\text{\AA}$. The calculated D is presented in Fig. 5(b) showing that the effective degeneracy is also maximized at this point. The

critical value of U_c (Fig. 5(c)) exhibits the same trend. Our results altogether indicate that the metallicity is enhanced due to orbital fluctuations in the vicinity to the degeneracy maximum point (For more details, see Supplemental Material [14]).

Importantly, this fluctuation overcomes the effect of reduced bandwidth, thereby triggering the phase transition. The bandwidth is monotonically decreased; see Fig. 5(b), clearly indicating that the competition between metallic and insulating phase is primarily governed by ‘degeneracy’. In the current case, so-called ‘strain engineering’ does not just control the bandwidth, but simultaneously change D , and importantly, the governing parameter is (effective) degeneracy. Obviously, the other possibilities such as ‘dimensionality’ and ‘filling’ control MIT are not relevant here.

As often being the case, this MIT is accompanied by magnetic transition at low temperature. As shown in Fig. 5(a), different magnetic phases are stabilized as a function of in-plane lattice constant. While the two end members of this phase diagram (*i.e.*, FM-I and AFM-I) have been reported previously by GGA+ U calculation [35], the PM-I phase at the degeneracy maximum point is first identified in the current DMFT study.

Summary We introduced a new measure of degeneracy, which estimates ‘effective’ degeneracy relevant to MIT. This quantity denoted by D can be easily calculated and is generally applicable to any real multi-orbital systems for which quantifying the degree of degeneracy is often hampered by the complicated band structures. By applying D to $3d$, $4d$, and $5d$ TMO, we show that this newly-introduced quantity works well to describe the electronic behavior as a function of external and internal parameters. In particular, we show that the effective degeneracy plays together with bandwidth change in the thickness-dependent transition of SRO-113 and that the ‘relativistic’ effect by SOC in the SIO-214 gap formation is primarily to lift degeneracy rather than to reduce bandwidth. From the strain dependent phase diagram of LTO/LAO superlattice, we suggest a novel ‘degeneracy control’ MIT. While ‘effective degeneracy’ is not the only component to describe MIT, our examples clearly show that this new quantity provides useful information which cannot be captured by other conventional quantities such as bandwidth and filling.

We thank A. T. Lee, H.-S. Kim, and S. W. Jang for technical helps. J.-H.S, S.R. and M.J.H were supported by Basic Science Research Program through the National Research Foundation of Korea (NRF) funded by the Ministry of Education (2018R1A2B2005204). The computing resource is supported by National Institute of Supercomputing and Networking / Korea Institute of Science and Technology Information with supercomputing resources (KSC-2015-C3-042).

-
- * mj.han@kaist.ac.kr
- [1] M. Imada, A. Fujimori, and Y. Tokura, *Rev. Mod. Phys.* **70**, 1039 (1998).
 - [2] E. Pavarini, S. Biermann, A. Poteryaev, A. I. Lichtenstein, A. Georges, and O. K. Andersen, *Phys. Rev. Lett.* **92**, 176403 (2004).
 - [3] Z. Zhong, M. Wallerberger, J. M. Tomczak, C. Taranto, N. Parragh, A. Toschi, G. Sangiovanni, and K. Held, *Phys. Rev. Lett.* **114**, 246401 (2015).
 - [4] A. Georges, L. de’ Medici, and J. Mravlje, *Annu. Rev. Condens. Phys.* **4**, 137 (2013).
 - [5] M. A. Hossain, B. Bohnenbuck, Y. D. Chuang, M. W. Haverkort, I. S. Elfimov, A. Tanaka, A. G. Cruz Gonzalez, Z. Hu, H.-J. Lin, C. T. Chen, R. Mathieu, Y. Tokura, Y. Yoshida, L. H. Tjeng, Z. Hussain, B. Keimer, G. A. Sawatzky, and A. Damascelli, *Phys. Rev. B* **86**, 041102 (2012).
 - [6] T. F. Qi, O. B. Korneta, S. Parkin, L. E. De Long, P. Schlottmann, and G. Cao, *Phys. Rev. Lett.* **105**, 177203 (2010).
 - [7] W. Brzezicki, A. M. Oleś, and M. Cuoco, *Phys. Rev. X* **5**, 011037 (2015).
 - [8] J. Zaanen, G. A. Sawatzky, and J. W. Allen, *Phys. Rev. Lett.* **55**, 418 (1985).
 - [9] D. J. Thouless, M. Kohmoto, M. P. Nightingale, and M. den Nijs, *Phys. Rev. Lett.* **49**, 405 (1982).
 - [10] M. Z. Hasan and C. L. Kane, *Rev. Mod. Phys.* **82**, 3045 (2010).
 - [11] X.-L. Qi and S.-C. Zhang, *Rev. Mod. Phys.* **83**, 1057 (2011).
 - [12] F. Aryasetiawan, M. Imada, A. Georges, G. Kotliar, S. Biermann, and A. I. Lichtenstein, *Phys. Rev. B* **70**, 195104 (2004).
 - [13] S. W. Jang, H. Sakakibara, H. Kino, T. Kotani, K. Kuroki, and M. J. Han, *Scientific Reports* **6**, 33397 (2016).
 - [14] Supplemental Material.
 - [15] D. Toyota, I. Ohkubo, H. Kumigashira, M. Oshima, T. Ohnishi, M. Lippmaa, M. Takizawa, A. Fujimori, K. Ono, M. Kawasaki, and H. Koinuma, *Appl. Phys. Lett.* **87**, 162508 (2005).
 - [16] J. Xia, W. Siemons, G. Koster, M. R. Beasley, and A. Kapitulnik, *Phys. Rev. B* **79**, 140407 (2009).
 - [17] G. Koster, L. Klein, W. Siemons, G. Rijnders, J. S. Dodge, C.-B. Eom, D. H. A. Blank, and M. R. Beasley, *Rev. Mod. Phys.* **84**, 253 (2012).
 - [18] K. Ishigami, K. Yoshimatsu, D. Toyota, M. Takizawa, T. Yoshida, G. Shibata, T. Harano, Y. Takahashi, T. Kadono, V. K. Verma, V. R. Singh, Y. Takeda, T. Okane, Y. Saitoh, H. Yamagami, T. Koide, M. Oshima, H. Kumigashira, and A. Fujimori, *Phys. Rev. B* **92**, 064402 (2015).
 - [19] Y. J. Chang, C. H. Kim, S.-H. Phark, Y. S. Kim, J. Yu, and T. W. Noh, *Phys. Rev. Lett.* **103**, 057201 (2009).
 - [20] L. Si, Z. Zhong, J. M. Tomczak, and K. Held, *Phys. Rev. B* **92**, 041108 (2015).
 - [21] S. Rye and M. J. Han, *Sci. Rep.* **7**, 4635 (2017).
 - [22] B. J. Kim, H. Ohsumi, T. Komesu, S. Sakai, T. Morita, H. Takagi, and T. Arima, *Science* **323**, 1329 (2009).
 - [23] B. J. Kim, H. Jin, S. J. Moon, J.-Y. Kim, B.-G. Park, C. S. Leem, J. Yu, T. W. Noh, C. Kim, S.-J. Oh, J.-H.

- Park, V. Durairaj, G. Cao, and E. Rotenberg, *Phys. Rev. Lett.* **101**, 076402 (2008).
- [24] R. Arita, J. Kuneš, A. V. Kozhevnikov, A. G. Eguiluz, and M. Imada, *Phys. Rev. Lett.* **108**, 086403 (2012).
- [25] A. Yamasaki, S. Tachibana, H. Fujiwara, A. Higashiya, A. Irizawa, O. Kirilmaz, F. Pfaff, P. Scheiderer, J. Gabel, M. Sing, T. Muro, M. Yabashi, K. Tamasaku, H. Sato, H. Namatame, M. Taniguchi, A. Hloskovskyy, H. Yoshida, H. Okabe, M. Isobe, J. Akimitsu, W. Drube, R. Claessen, T. Ishikawa, S. Imada, A. Sekiyama, and S. Suga, *Phys. Rev. B* **89**, 121111 (2014).
- [26] H. Zhang, K. Haule, and D. Vanderbilt, *Phys. Rev. Lett.* **111**, 246402 (2013).
- [27] D. Hsieh, F. Mahmood, D. H. Torchinsky, G. Cao, and N. Gedik, *Phys. Rev. B* **86**, 035128 (2012).
- [28] C. Martins, M. Aichhorn, L. Vaugier, and S. Biermann, *Phys. Rev. Lett.* **107**, 266404 (2011).
- [29] T. Sato, T. Shirakawa, and S. Yunoki, *Phys. Rev. B* **91**, 125122 (2015).
- [30] A. Georges, S. Florens, and T. Costi, *J. Phys. IV France* **114**, 165 (2004).
- [31] K. Ishii, I. Jarrige, M. Yoshida, K. Ikeuchi, J. Mizuki, K. Ohashi, T. Takayama, J. Matsuno, and H. Takagi, *Phys. Rev. B* **83**, 115121 (2011).
- [32] H. Watanabe, T. Shirakawa, and S. Yunoki, *Phys. Rev. Lett.* **105**, 216410 (2010).
- [33] S. Mohapatra, J. van den Brink, and A. Singh, *Phys. Rev. B* **95**, 094435 (2017).
- [34] S. S. A. Seo, M. J. Han, G. W. J. Hassink, W. S. Choi, S. J. Moon, J. S. Kim, T. Susaki, Y. S. Lee, J. Yu, C. Bernhard, H. Y. Hwang, G. Rijnders, D. H. A. Blank, B. Keimer, and T. W. Noh, *Phys. Rev. Lett.* **104**, 036401 (2010).
- [35] A. T. Lee and M. J. Han, *Phys. Rev. B* **89**, 115108 (2014).
- [36] M. Daghofer, K. Wohlfeld, A. M. Oleś, E. Arrigoni, and P. Horsch, *Phys. Rev. Lett.* **100**, 066403 (2008).
- [37] Y. Weng and S. Dong, *Journal of Applied Physics* **117**, 17C716 (2015).

Supplemental Material : Quantified Degeneracy and Metal-Insulator Transition in Complex Transition-metal Oxides

Jae-Hoon Sim¹, Siheon Ryee¹, Hunpyo Lee², and Myung Joon Han^{1,3*}

¹*Department of Physics, Korea Advanced Institute of
Science and Technology (KAIST), Daejeon 34141, Korea*

²*Department of General Studies, Kangwon National University,
Samcheok-si, Kangwon-do 25913, Korea and*

³*KAIST Institute for the NanoCentury,
Korea Advanced Institute of Science and Technology, Daejeon 34141, Korea*

(Dated: July 4, 2021)

I. COMPUTATION METHOD

First-principles electronic structure calculations have been carried out based on DFT (density functional theory) within GGA-PBE (generalized gradient approximation as parameterized by Perdew-Burke-Ernzerhof)¹. We used two different software package, namely, ‘VASP’² for ruthenates and titanates and ‘OpenMX’³⁻⁶ for iridates and titanates. In SRO-113 calculation, $8 \times 8 \times 2$ \mathbf{k} -points have been taken and the slab geometries with a vacuum thickness of $\geq 15 \text{ \AA}$ considered. The force criterion for structural optimizations was 1 meV/\AA . Other details can be found in our previous publication of SRO-113 thin film⁷. For SIO-214, we used DFT+ U method^{3,8} to take on-site correlation into account with $8 \times 8 \times 4$ \mathbf{k} -points. Critical value of U_c was defined as the smallest U at which the gap is opened. SOC is treated within a fully relativistic j -dependent potential. For LTO/LAO superlattice, we used $7 \times 7 \times 3$ \mathbf{k} -points and the optimized lattice structure obtained in our previous study⁹. To describe the electronic correlation, single-site DMFT has been adopted. Three maximally localized Wannier functions (WFs) are constructed for each Ti site starting from the initial projections onto atomic Ti- t_{2g} orbitals^{10,11}. This Hamiltonian serves as the non-interacting H_0 for the multiband Hubbard Hamiltonian $H = H_0 + H_{\text{int}}$. The interaction part is expressed in the Slater-Kanamori form $H_{\text{int}} = \sum_i h_{i,\text{int}}$;

$$h_{i,\text{int}} = \sum_{\alpha} U n_{i\alpha\uparrow} n_{i\alpha\downarrow} + \sum_{\alpha \neq \beta} U' n_{i\alpha\uparrow} n_{i\beta\downarrow} \quad (1)$$

$$+ \sum_{\alpha \neq \beta, \sigma} (U' - J_H) n_{i\alpha\sigma} n_{i\beta\sigma}, \quad (2)$$

where U , U' , and J_H refers to the intra-orbital, inter-orbital, and Hund interaction, respectively, with $U' = U - 2J$ and $J_H/U = 0.14$ ¹². The Hamiltonian is solved within single-site DMFT (dynamical mean-field theory) by employing a hybridization expansion continuous-time quantum Monte Carlo (CT-QMC) algorithm implemented in ALPS library¹³⁻¹⁵. In this procedure, the local Green’s functions is calculated using momentum-independent self-energy:

$$G_{\text{loc}}(i\omega_n) = \frac{1}{N_k} \sum_{\mathbf{k}} \frac{1}{i\omega_n + \mu - H_0(\mathbf{k}) - \Sigma(i\omega_n)}, \quad (3)$$

where $H_0(\mathbf{k})$ and $\Sigma(i\omega_n)$ are given by 12×12 matrices. Self-energy is decomposed into 6×6 matrices corresponding to two Ti sites, $\Sigma(i\omega_n) = \Sigma_{\text{Ti}(1)}(i\omega_n) \oplus \Sigma_{\text{Ti}(2)}(i\omega_n)$. The self-energy in the real frequency domain is obtained from the matsubara Green’s functions and self-energy

by analytic continuation using the maximum entropy method (MEM)^{16,17}. The stability is also checked by using stochastic method.

II. SUPPLEMENTARY TABLE: THE CALCULATED VALUES OF D AND $S_{n\alpha}$

	control parameter	D	S_1	S_2	S_3
SRO-113	+2%	4.949	0.941	0.987	0.494
	0%	5.255	0.977	0.974	0.676
	-2%	5.416	0.959	0.956	0.793
SIO-214	0.000 eV	3.490	0.784	0.782	0.179
	0.479 eV	2.855	0.980	0.394	0.053
LTO/LAO	3.905 Å	3.751	0.806	0.663	0.405
	4.040 Å	3.781	0.780	0.650	0.441
	4.060 Å	3.805	0.787	0.636	0.478
	4.100 Å	3.697	0.857	0.547	0.445

TABLE I: The calculated D and S_μ for three different systems considered in this study. Note that the states $|S_{1,2,3}\rangle$ are obtained from the diagonalization of the number operators, and therefore do not exactly correspond to any of conventional symmetry states. The ‘control parameters’ refers to the value of strain, the SOC strength (λ), and the in-plane lattice constant for SRO-113, SIO-214, and LTO/LAO, respectively.

III. SUPPLEMENTARY FIGURE: STRAIN DEPENDENT DOS FOR LTO/LAO

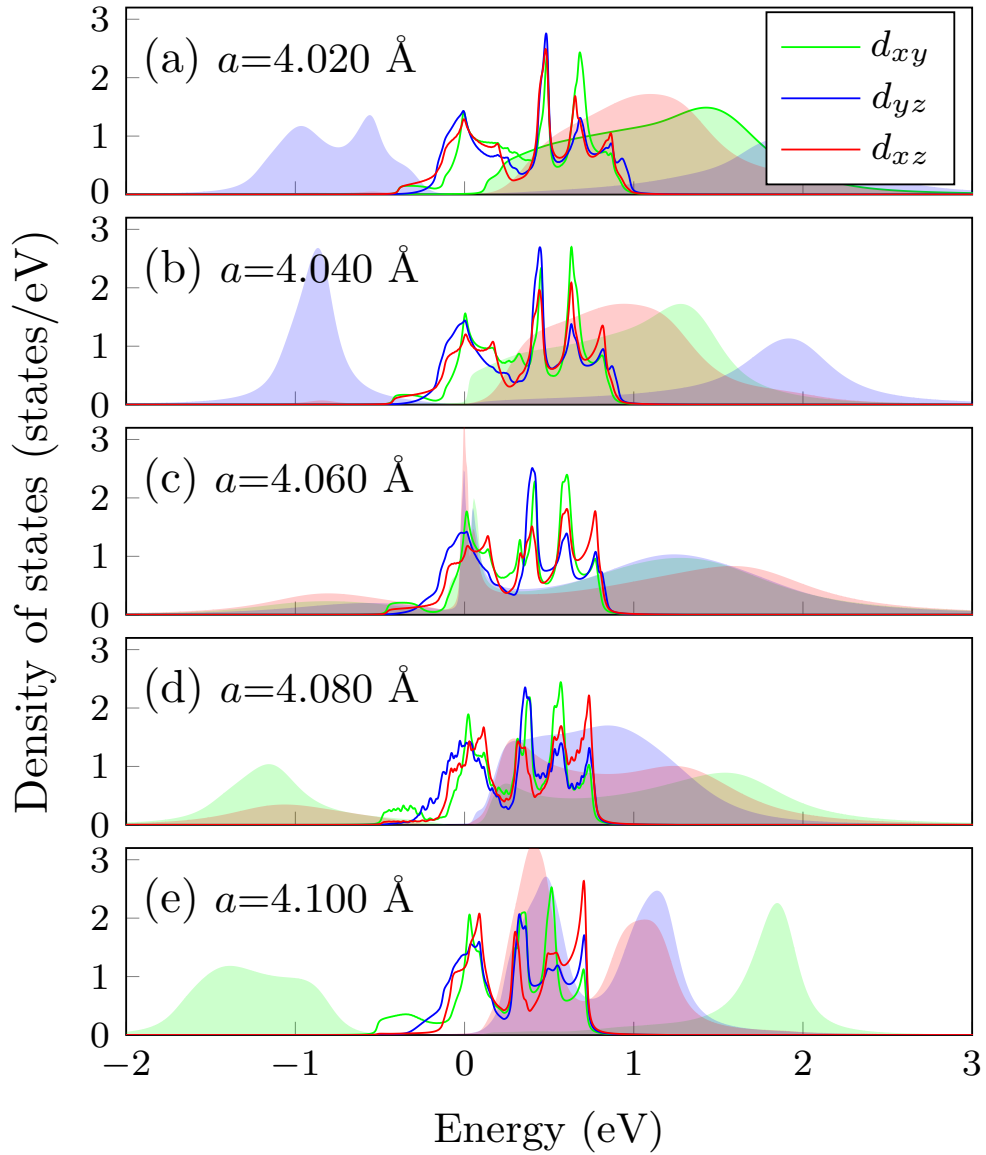


FIG. 1: The orbital-resolved spectral functions of one of Ti sites as a function of in-plane lattice constant. $U=0$ and $U=3$ eV results are presented with the lines and the shaded area, respectively. The d_{xy} , d_{yz} and d_{zx} is represented by green, blue, and red colors, respectively. The Fermi level is set to 0.

IV. PHYSICAL MEANING OF D

D is expressed with binary entropy of the eigenvalues of on-site number matrix, $S(n_\mu) = -n_\mu \log_2 n_\mu - (1-n_\mu) \log_2 (1-n_\mu)$. Since n_μ can be interpreted as a probability that the orbital μ is occupied, the probability $P_{\text{loc}}(\{n_\mu\})$ of the local micro-states $n_\mu \in \{\text{occupied, unoccupied}\}$ can be written as $\prod_\mu^{\text{occ}} n_\mu \prod_\nu^{\text{unocc}} (1 - n_\nu)$. Here the ‘correlations’ between electrons are not taken into account which is consistent with that D is calculated within the ‘non-interacting’ Hamiltonian. From the additivity of logarithmic function,

$$D = S(\Pi_\mu n_\mu) = S(P_{\text{loc}}(\{n_\mu\})) = S_{\text{vN}}(\hat{\rho}_0), \quad (4)$$

where $S_{\text{vN}}(\hat{\rho}_0) = -\text{Tr}(\hat{\rho}_0 \log \hat{\rho}_0)$ is the von Neumann entropy for the quantum mechanical density matrix $\hat{\rho}_0 = \text{Tr}_{i \neq 0} |\Psi\rangle\langle\Psi|$ at the local site $i = 0$ and ground state $|\Psi\rangle$. The relation between D and the entropy (Eq. (4)) is thus quite natural.

Note that the larger D implies the larger fluctuation or entropy of a system. As obvious from its entropy-like definition, D measure the on-site electron fluctuations between different orbitals which suppresses the tendency^{18,19}.

Not surprisingly, the physical meaning of D is multi-fold being related to other more ‘conventional’ quantities. As discussed in the main manuscript, D carries the information of band fillings as well as the (mere) degeneracy and entropy relevant to metal-insulator transition^{18,19}. Further, D can conceptually be extended and closely related to ‘entanglement entropy’ in a certain parameter regime²⁰. It seems a promising future direction to explore the physical implication of D .

¹ J. P. Perdew, K. Burke, and M. Ernzerhof, Phys. Rev. Lett. **77**, 3865 (1996).

² G. Kresse and D. Joubert, Phys. Rev. B **59**, 1758 (1999).

³ M. J. Han, T. Ozaki, and J. Yu, Phys. Rev. B **73**, 045110 (2006).

⁴ <http://www.openmx-square.org>.

⁵ T. Ozaki and H. Kino, Phys. Rev. B **69**, 195113 (2004).

⁶ T. Ozaki, Phys. Rev. B **67**, 155108 (2003).

⁷ S. Ryee and M. J. Han, Sci. Rep. **7**, 4635 (2017).

- ⁸ S. L. Dudarev, G. A. Botton, S. Y. Savrasov, C. J. Humphreys, and A. P. Sutton, Phys. Rev. B **57**, 1505 (1998).
- ⁹ A. T. Lee and M. J. Han, Phys. Rev. B **89**, 115108 (2014).
- ¹⁰ N. Mazari and D. Vanderbilt, Phys. Rev. B **56**, 12847 (1997).
- ¹¹ I. Souza, N. Mazari, and D. Vanderbilt, Phys. Rev. B **65**, 035109 (2001).
- ¹² E. Pavarini, S. Biermann, A. Poteryaev, A. I. Lichtenstein, A. Georges, and O. K. Andersen, Phys. Rev. Lett. **92**, 176403 (2004).
- ¹³ F. Alet, P. Dayal, A. Grzesik, A. Honecker, M. Körner, A. Läuchli, S. R. Manmana, I. P. McCulloch, F. Michel, R. M. Noack, G. Schmid, U. Schollwck, F. Stekli, S. Todo, S. Trebst, M. Troyer, P. Werner, and S. Wessel, J. Phys. Soc. Jpn. Suppl. **74**, 30 (2005).
- ¹⁴ E. Gull, A. J. Millis, A. I. Lichtenstein, A. N. Rubtsov, M. Troyer, and P. Werner, Rev. Mod. Phys. **83**, 349 (2001).
- ¹⁵ E. Gull, P. Werner, S. Fuchs, B. Surer, T. Pruschke, and M. Troyer, Computer Physics Communications **182**, 1078 (2011).
- ¹⁶ M. Jarrell and J. E. Gubernatis, Physics Reports **269**, 133 (1996).
- ¹⁷ O. Gunnarsson, M. W. Haverkort, and G. Sangiovanni, Phys. Rev. B **81**, 155107 (2010).
- ¹⁸ S. Florens, A. Georges, G. Kotliar, and O. Parcollet, Phys. Rev. B **66**, 205102 (2002).
- ¹⁹ O. Gunnarsson, E. Koch, and R. M. Martin, Phys. Rev. B **54**, R11026 (1996).
- ²⁰ M. A. Nielsen and I. L. Chuang, *Quantum Computation and Quantum Information* (Cambridge University, 2010).